Polymer 51 (2010) 2106–2111

Contents lists available at ScienceDirect

Polymer

journal homepage: www.elsevier.com/locate/polymer

Heat capacities of both PMMA stereomers: Comparison between atomistic simulation and experimental data

Armand Soldera [a,*], Noureddine Metatla [a], Alexandre Beaudoin [a], Sylvere Said [b], Yves Grohens [b]

[a] Department of Chemistry, Université de Sherbrooke, Sherbrooke, Québec J1K 2R1, Canada
[b] Laboratoire d'ingénierie des matériaux de Bretagne (LIMATB), Université de Bretagne Sud, Centre de Recherche, rue Sainte Maudé, 56321 Lorient Cédex, France

ARTICLE INFO

Article history:
Received 21 January 2010
Received in revised form
26 February 2010
Accepted 1 March 2010
Available online 7 March 2010

Keywords:
Specific heat capacity
Molecular dynamics
Flex bonds

ABSTRACT

The domains of time and space generally covered by full atomistic simulation (AS) to represent the glass transition temperature, T_g, are very small. Physical interpretations of the phenomena occurring at this transition are inevitably limited. To specifically address such limitation, behavior of the heat capacity that accounts for the freezing of the degrees of freedom as temperature is decreased, is investigated. The selected polymer is poly(methyl methacrylate) since it offers the opportunity to exhibit a different T_g according to the tacticity of its chain. AS and experimental data are thus compared to a theoretical model that takes into account three contributions to the leap in the heat capacity occurring at T_g. The comparison discloses that an excellent agreement is obtained between simulated and experimental contributions from vibrations and free volume. However, from an AS viewpoint changes in the conformation weakly contribute to this leap. Despite this discrepancy local contributions to the glass transition as predicted by atomistic simulation, are sufficient to determine T_g.

1. Introduction

From an experimental viewpoint, the glass transition in polymers or glass formers is usually characterized by dramatic changes in the viscosity and the relaxation time by nearly 10 decades, as the temperature is lowered [1,2]. These variations occur over a small range of temperatures, about a dozen of degrees, for fragile glass formers, yielding a glassy material at a temperature defined as the glass transition temperature, T_g. To describe the vast domain of relaxation times involved during this small range of temperatures, molecular modelling has been shown to be a beneficial tool to corroborate existing theories [3]. In fact, among the different kinds of simulations, the coarse-grained approach remains the most appropriate technique to deal with the time spreading phenomenon. Alternatively, atomistic simulation (AS) is more appropriate to treat the effect of small local variations in the atomistic architecture at the repeat unit scale (side chain, tacticity, head-to-head or tail, etc.) on the value of T_g [4,5]. Despite the small domain of time usually covered by AS, we have shown that transition temperatures that are usually related to T_gs can be determined using this approach [6]. To compensate for non-equilibrium structures, a specific procedure based on an appropriate selection of configurations (10) followed by an optimization process, yielded T_gs (T_g^{AS}) that are related to experimental T_gs ($T_g^{exp.}$) by the well-established Williams-Landel-Ferry (WLF) equation: the fitted universal parameters C_1 and C_2 for a series of nine vinylic polymers were found to be comparable to the experimentally measured universal constants [7]. The intimate connection between T_g^{AS} and $T_g^{exp.}$ allowed for a correlation of AS data with actual theories on the glass transition [8]. Simulation data have thus been confronted with the Adam–Gibbs model that introduces the concept of the cooperative rearranging region (CRR) [9]. A relation between the effective activation energy appearing in the Vogel-Fulcher-Tamman (VFT) equation [10] and T_g was established, revealing the importance of the correlation between both the side chain and the backbone in vinylic polymers to the value of T_g, thus confirming experimental [11] and simulated results [12,13]. It can then be argued that due to these accurate results AS is perfectly adapted to describe the glass transition, and thus to usefully complement higher-levels of approximation simulation, theories, and experiments. Nevertheless the restricted description of the phase space (domain of times covered by AS, number of limited points in the configurational space) limits the use of AS to give an accurate portrait of the glass transition phenomenon. To specifically address this limitation, poly(methyl methacrylate) (PMMA) is used since it offers the particular opportunity to exhibit different T_gs according to the tacticity of its chain [14]. From an AS viewpoint, this fact is of particular significance since the same force field parameters are

* Corresponding author. Tel.: +1 819 821 7650; fax: +1 819 821 8017.
E-mail address: armand.soldera@usherbrooke.ca (A. Soldera).

0032-3861/$ – see front matter © 2010 Elsevier Ltd. All rights reserved.
doi:10.1016/j.polymer.2010.03.003

employed to treat both configurations [6]. Once the difference in T_gs between the two chain tacticities of PMMA is correctly depicted, observed differences are attributed to changes in molecular characteristics only [15]. This paper is thus aimed to explicitly show the domain of relevance of AS in the description of this perplexing transition in PMMA by directly comparing AS results with experimental data.

As the polymeric system crosses the glass transition upon cooling, specific degrees of freedom are frozen, and this phenomenon is characterized by plotting the change in heat capacity with respect to the temperature (Fig. 1). The spreading of the heat capacity discontinuity at the glass transition is in agreement with the fact that it is not a real second order transition, following Ehrenfest nomenclature. According to the Gibbs–DiMarzio model, it becomes a true second order transition at an infinitely low cooling rate [16]. This leap in the heat capacity corresponds to a progressive freezing of the degrees of freedom along the polymer chain [17]. Its interpretation by differentiating several contributions that make the polymer a glass, is still a source of debate in the literature [18,19]. To strictly compare the behavior of experimental and simulated heat capacities with respect to the temperature, the model of three contributions was considered [16]. The purpose of the study reported in this paper is then to extract from the resulting differences the limits of full atomistic simulation in describing the glass transition phenomenon.

2. Simulation details and experimental section

2.1. Simulation details

Complete details of simulation reported in this text are treated in previous articles [20–22]; relevant information and specific distinctions are presented herein. Simulations described in this paper have been carried out with PMMA chains of 300 RUs length. For each chain, five configurations have been selected, and their generation inside the periodic boundary conditions box followed the self-avoiding walk procedure implemented in the Amorphous_Cell© code in the Accelrys Materials Studio environment [23,24]. A relaxation procedure was then initiated with a heating of the system from 100 K to 800 K with 50 K steps, and a molecular dynamics (MD) simulation duration of 1.1 ns (0.1 ns in the NVT ensemble, followed by 1 ns in the NPT ensemble at each step). The cooling process was thereafter carried out by decreasing the temperature from 800 K to 240 K by 20 K steps, with MD duration of 3 ns at each step. Such cooling rate allowed for a gradual elimination of the entropic contribution. The OPLS (Optimized Potentials for Liquid Simulations) force field was employed [25]. All the MD simulations have been carried out using the Verlet-leapfrog integration algorithm with a 1 fs integration time step [26]. During MD simulations the Berendsen thermostat and barostat were used to keep the system at prescribed temperatures and pressures, respectively [27]. The cut-off procedure with a 10 Å cut-off and a spline function to bring the potential to zero, has been used to compute the Van der Wals interactions, while the Ewald summation method [28] was employed to calculate the electrostatic interactions. A uniform hydrostatic compression was carried out in order to get configurations in a potential well [22]. It was these configurations that were used to compute reproducible T_g using the LAMMPS package [29].

2.2. Determination of the simulated T_g

Once a conformation of the PMMA chain has been optimized according to a hydrostatic compression procedure described in ref. [22], a simulated dilatometric procedure was carried out, cooling the system from 800 K to 240 K by 20 K steps. The system remained at each temperature during 5 ns. During this cooling process, the specific volume, i.e. the inverse density, was calculated at each temperature. The departure from a linear relationship between the specific volume and the temperature yielded the value of the T_g which corresponds to the transition from the rubbery to the vitreous phases, as shown in Fig. 2.

2.3. Determination of simulated specific heat capacities

C_v or C_p have been extracted from molecular dynamics trajectories using fluctuations properties [30] as shown in Eqs. (1) and (2), respectively.

$$C_v^{AS} = \langle \overline{C_v} \rangle = \left\langle \frac{\overline{E^2} - \overline{E}^2}{k_B T^2} \right\rangle \quad (1)$$

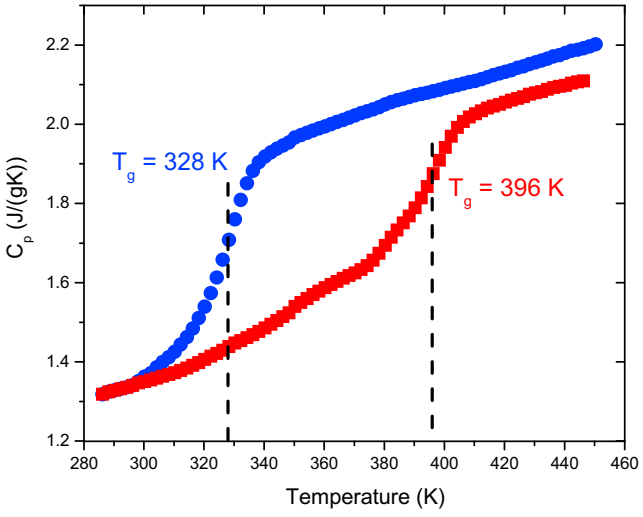

Fig. 1. Experimental heat capacity of i-PMMA (●) and s-PMMA (■) versus temperature.

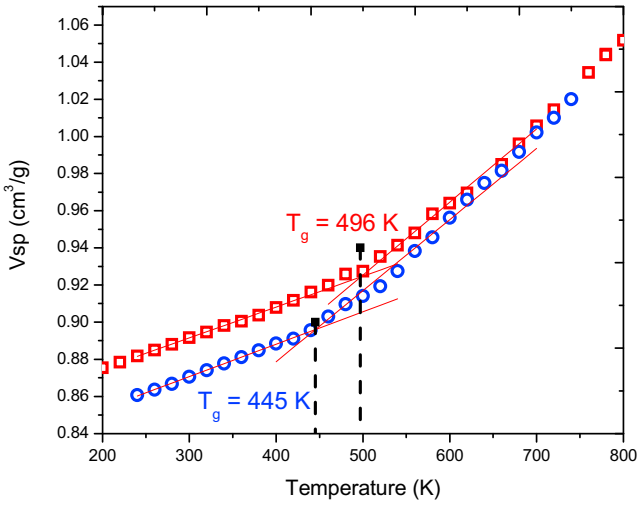

Fig. 2. Simulated dilatometry, i.e. specific volume (V_{sp}) versus the temperature, of i-PMMA (○) and s-PMMA (□).

$$C_p^{AS} = \left\langle \overline{C_p} \right\rangle = \left\langle \frac{\overline{H^2} - \overline{H}^2}{k_B T^2} \right\rangle \quad (2)$$

where E and H are the internal energy and the enthalpy of the system, respectively; T is the temperature; k_B is the Boltzmann constant; the upper bar indicates a time average; and the brackets describe the fact that the average is taken over the 5 optimized configurations for which simulated T_g has been derived; the superscript AS stands for atomistic simulation. To specifically compare simulation with experiment, C_p^{AS} is used. The enthalpy at a particular time t is computed following:

$$H(t) = E(t) + \overline{p}V(t) \quad (3)$$

where $\overline{p}$ corresponds to the average of pressure over time along one molecular dynamics trajectory since simulations are carried out in the NPT ensemble.

Another way to extract average values of C_p from AS, instead of using Eq. (2), is to determine it from the slope of the enthalpy with respect to the temperature. This approach is thorny since the thermodynamic limit is not reached: number of points in the phase space and time of the simulation do not allow the equality between the computed average energy, $\langle E \rangle$, and the internal energy U. Thus Eq. (2) is used to compute the heat capacity.

2.4. Determination of the experimental heat capacities ($C_p^{exp.}$)

For a better comparison between experimental and simulated data, stereoregular PMMAs with high tacticity contents and with a number of RUs approaching 300 were investigated. They were purchased from Polymer Source Inc., and used as received. Their properties are shown in Table 1. The determination of the specific heat capacity was performed on a Mettler Toledo DSC using sapphire as a standard. The calibration of the DSC has been monitored with indium and tin standards. The same weight for each sample, 9 mg, was used for all experiments. The cooling and heating cycles were realized under nitrogen, with a scanning rate of 5 °C/min and 10 °C/min, respectively to avoid any temperature gradient within the samples. Experimentally, the domain of temperatures that was covered ranged between $T_g - 60$ °C and $T_g + 60$ °C, enabling an accurate determination of the solid and liquid $C_p(T)$ around the glass transition. All the samples have been annealed prior to the measurements at 200 °C for 5 min in order to erase any thermal history and to minimize the thermal resistance at the contact between the polymer and the pan. The measurements were carried out during the second cooling with a scanning rate of 5 °C/min. Three scans were completed for reproducibility. The reported heat capacity values thus correspond to the average taken over these runs.

3. Results and discussion

3.1. Specific heat capacity curves

Experimental (M_w ~30,000 g/mol) and simulated (300 RUs) heat capacities for both PMMA tacticities were determined and are shown in Figs. 1 and 3, respectively. The values of T_g, the specific heat capacity jump at T_g, as well as expansion coefficient at T_g, $\Delta\alpha$, are compiled in Table 2. From 460 K down to around 290 K for experimental curves, and from 200 K up to 800 K for computed curves, below T_g, the temperature dependence of $C_p^{exp.}$ and C_p^{AS} is most often linear. In the glassy state, $C_p(T)$ is mainly determined by the vibrational spectra of the polymer that is composed of the lattice vibrations predominant at low temperature, characteristic vibrations resulting from the normal modes of an RU, and librational motions inside a rotameric potential well. The similar behavior of both heat capacities with respect to the temperature is in agreement with the reliable calculation of the infrared spectra of PMMA [31].

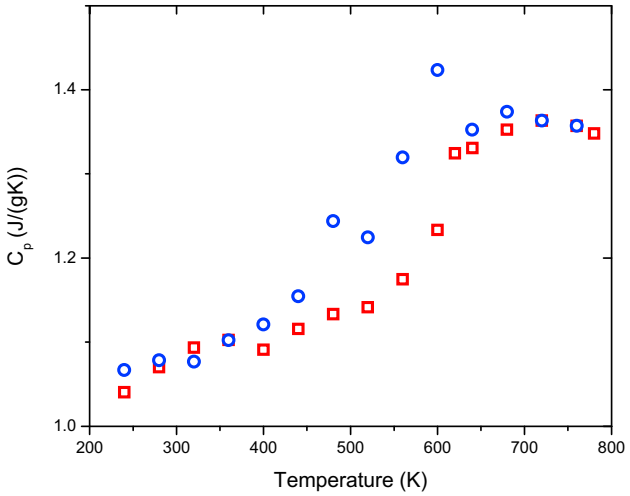

Fig. 3. Simulated heat capacity versus the temperature, of i-PMMA (○) and s-PMMA (□) versus temperature.

Another point of agreement is the fact that in both cases the T_g for the isotactic configuration is lower than the T_g of the syndiotactic configuration. In this case experimental data and simulated dilatometry are in agreement (Table 2). Despite these consistencies between experimental and simulated curves, divergences are clearly observed. The search for the origin of these discrepancies is at the heart of this study. From the simulation perspective, they can be grouped into three topics:

(1) higher values of T_g;
(2) a broader transition temperature range;
(3) a lower difference in the heat capacity between the liquid and glass states.

These three differences are discussed in the following paragraph.

3.2. Glass transition temperature

It is argued that discrepancies between simulated and experimental values of T_g stem from the important difference in the cooling rates. The simulated cooling rate is on the order of 10^{11} times higher than the experimental one. The impact of this very

Table 1
Characteristics of experimental PMMAs used in this study.

	M_n, kg/mol	M_w, kg/mol	M_w/M_n	Tacticity content, %
i-PMMA	29	36.5	1.25	>91
s-PMMA	30	37.5	1.25	>79

Table 2
Experimental (30,000 g/mol) and simulated (300 RUs) values used to compute the different contribution to the leap in the heat capacity.

PMMA	$T_g(K)$		$\Delta\alpha(K^{-1})$		$C_p(T_{g^-})$ (J g^{-1}K^{-1})	
	Exp.	AS	Exp.	AS	Exp.	AS
Iso	328	445	3.8×10^{-4}	2.2×10^{-4}	1.4	1.12
Syn	396	497	3.1×10^{-4}	2.0×10^{-4}	1.66	1.14

high cooling rate on the determination of T_g has been analyzed by Metatla and Soldera in a two-step approach [7]. A systematic optimization procedure was first undertaken for a series of vinylic polymers: an appropriate selection of the configurational space is followed by a relaxation procedure based on the use of a simulated annealing and a uniform hydrostatic compression [22]. The simulated dilatometry applied to these systems yields reproducible values of T_gs, which are linked to experimental T_gs by a linear equation. This relationship was then investigated for two other cooling rates. The investigation of the dependence of the T_gs with the cooling rates showed that they obeyed the time–temperature equivalence depicted by the well-established William-Landel-Ferry (WLF) equation [7]. Addressing simulated T_gs using additional cooling rates in order to verify the accuracy of this relationship is very time consuming. The use of a lower cooling rate was consequently applied to only one polymer, i-PMMA. The difference between the experimental and the simulated T_gs, ΔT_gs, was then added to the existing curve of ΔT_gs with respect to $\log_{10}(t/t_g)$. The C_1 and C_2 parameters in the WLF equation used to derive this curve stem from the fit performed with the higher cooling rates [7]: $C_1 = 16.7$ and $C_2 = 48$ K. The new point perfectly fits into the curve (Fig. 4), showing the capacity of AS to depict the glass transition within the WLF context. Despite the appropriateness of the procedure to correlate simulated and experimental T_gs, no information about the phenomenon generated at the glass transition can be gained only from simulated curves. A change in the free volume expansion is monitored only since WLF which depicts the change in the free volume as temperature is changed makes the link between experimental and simulated T_gs.

Due to the equivalence between simulated and experimental T_gs [7], a homothetic transformation of the origin along the abscissa axis in Figs. 1 and 3 was thus undertaken to match simulated and experimental T_gs of i-PMMA, yielding the curve in Fig. 5. From this Figure, the two other differences between experimental and simulated data previously quoted, are plainly revealed.

3.3. Broadening of the heat capacity at the glass transition

The cooling rate greatly affects the spreading of C_p at the experimental glass transition [32–34]. The procedure that has been

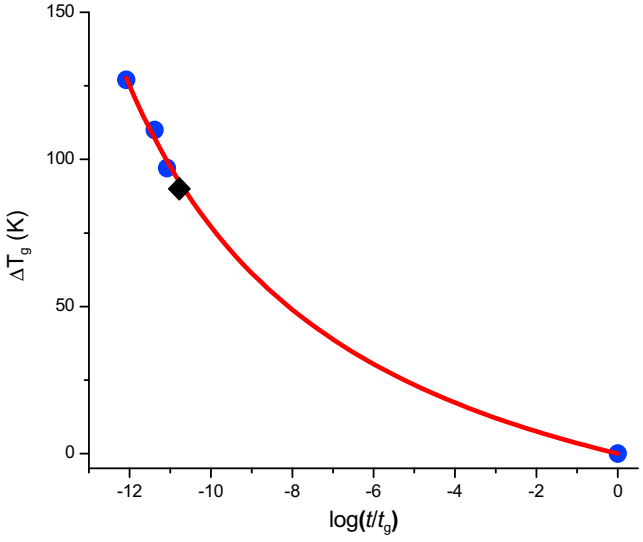

Fig. 4. Variation of the $\Delta T_g = T_g - T_g$(expt) for *i*-PMMA (●) with respect to $\log_{10}(t/t_g)$. The fitting curve of the WLF equation with $C_1 = 16.7$ and $C_2 = 48$ K is shown. The additional point (◆) corresponds to the value of T_g obtained with a cooling rate of 20 K/5 ns (2.4×10^{11} K/min).

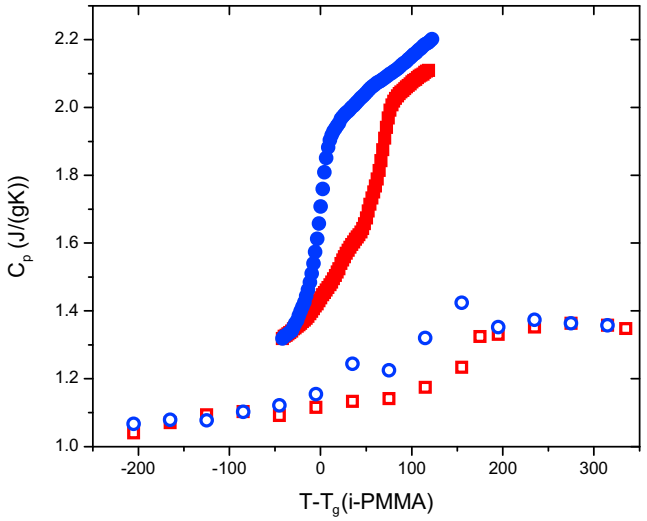

Fig. 5. Experimental (filled symbols) and simulated (empty symbols) heat capacities of i-PMMA (● and ○) and s-PMMA (■ and □) versus ($T - T_g$ (i-PMMA)).

used by scaling simulated T_gs at different cooling rates with experimental T_gs through the use of the WLF equation can no longer be employed [7]. In fact, the C_1 and C_2 parameters occurring in the WLF equation have to be determined at each temperature since the free volume varies with temperature [10]. A difference in the spreading has been observed between the simulated heat capacities computed at the different cooling rates. However, the difference is too small to ascertain that the cooling rate has an influence on the spreading of the simulated data. The reason for this small difference is due to the use of very high cooling rates on order of 10^{11} K/min. Based on these experimental observations, it is then argued that despite the non-demonstration of this influence from an AS viewpoint the very rapid cooling rate is responsible for the broadening observed for C_p.

3.4. Heat capacity discontinuity at the glass transition

To better understand the jump in the heat capacity that occurs at the glass transition, and to take into account the differences between experimental and simulated curves, the different contributions to $C_p(T)$ have to be examined. There are actually two main ways to describe this discontinuity. One method is to use the Tarasov function considering approximate group-vibrational spectra [35,36]. Due to the possibility of error associated with the fit of such a function to simulated data, another approach has been favored, and is outlined below.

The discontinuity in the heat capacity that occurs at the glass transition as the temperature is increased is principally due to the need of additional energy to create the necessary volume for larger amplitude motions, and vibrations. The model developed by DiMarzio and Dowell [37], which is an extension of the O'Reilly model [17] and Gibbs–DiMarzio theory [16], takes then into account three contributions that result from this need of volume expansion (Eq. (4)).

$$\Delta C = \Delta C_{\text{vib.}} + \Delta C_{\text{conf(vol.)}} + \Delta C_{\text{conf(shape)}} \tag{4}$$

where:

$\Delta C_{\text{vib.}}$ corresponds to the vibrational contribution;
$\Delta C_{\text{conf(vol.)}}$ is the configurational contribution resulting from the change in the volume expansion occurring at the glass transition region;

$\Delta C_{conf(shape)}$ is the configurational contribution resulting from the change in the shape occurring at the glass transition region.

In order to explicitly compare simulated and experimental behavior, heat capacities are reported with respect to $(T - T_g(\text{i-PMMA}))$ (Fig. 5). For C_p^{AS} errors are on order of $\pm 0.05\ \text{J g}^{-1}\ \text{K}^{-1}$. Between the experimental and simulated curves, a clear difference in the jump of the heat capacity is observed: $\Delta\Delta C = \Delta C_p^{exp.} - \Delta C_p^{AS} \approx 0.2\ \text{J g}^{-1}\ \text{K}^{-1}$. To reveal the factors that cause this difference, contribution of each term intervening in the total heat capacity (Eq. (4)) is specifically regarded. For each contribution, the derived relation is described in the following paragraphs [37], allowing for the determination of experimental and simulated values, and thus uncovering the discrepancies of simulation.

3.5. Vibrational contribution $\Delta C_{vib.}$

Vibrational contribution to the heat capacity leap is determined from the dilatometric curve and the graph of the heat capacity versus the temperature, and expressed in the following equation [37]:

$$\Delta C_{\text{vib.}} = 0.5 T \Delta\alpha C_p\left(T_{g^-}\right) \tag{5}$$

Where $C_p(T_{g^-})$ corresponds to the specific heat capacity in the glassy state below T_g, and computed from curves shown in Fig. 5 (values are shown in Table 2); $\Delta\alpha$ is the change in the expansion coefficient at T_g. This difference is directly obtained from the dilatometric curve (Fig. 1). Values of experimental and simulated $\Delta C_{\text{vib.}}$ are displayed in Table 3. A small difference is observed between experimental and simulated values of $\Delta C_{\text{vib.}}$ but this difference cannot explain the great difference in $\Delta\Delta C$. Despite a clear description of the stretching modes, the low frequency domain exhibits great discrepancies with the experimental infrared spectra. A deeper analysis will require the calculation of Einstein vibrations, and are beyond the topic of this text.

3.6. Volume expansion contribution $\Delta C_{conf(vol.)}$

Determination of the vibrational expansion contribution to the heat capacity jump directly stems from the dilatometric curve [37]:

$$\Delta C_{\text{conf(vol.)}} = 4RT\Delta\alpha(1 - 4.17T\Delta\alpha) \tag{6}$$

where R is the ideal gas constant. All the experimental and simulated values are displayed in Tables 2 and 3 for $\Delta C_{\text{conf(vol.)}}$.

Experimental and simulated values of $\Delta C_{\text{conf(vol.)}}$ are similar (Table 3). A small difference in simulated values between the two PMMA stereomers is observed, but could not be attributed to any difference in the T_gs since it is included within the standard mean deviation.

3.7. Shape contribution $\Delta C_{conf(shape)}$

Contrary to the two previous contributions to the heat capacity leap at T_g, the shape contribution cannot be directly determined from experimental or simulated curves. The variation in this specific heat capacity at T_g has been derived by Gibbs and DiMarzio [16]. It is inferred from the Rotational Isomeric State model of PMMA [38] considering two energy levels separated by E_{conf}; the higher in energy exhibiting a degeneracy of 2 corresponding to the g and g^- states.

$$\Delta C_{\text{conf(shape)}} = R\left(\frac{E_{\text{conf}}}{k_B T}\right)^2 f(1-f) \tag{7}$$

where f is the fraction of bonds in the g or g^- state:

$$f = \frac{2\exp.\left(\frac{-E_{\text{conf}}}{k_B T}\right)}{1 + 2\exp.\left(\frac{-E_{\text{conf}}}{k_B T}\right)} \tag{8}$$

Experimental investigation of $\Delta C_{\text{conf(shape)}}$ is first carried out. According to DiMarzio and Dowell, its contribution to the variation of the heat capacity at T_g has been set to 6 J/(flexible unit K), yielding $-E_{\text{conf}}/k_B T$ of 2.25 (Eq. (7)) [37]. Experimental measurements and simulation have shown that the two PMMA configurations exhibit different values of E_{conf} in agreement with the fact that a difference in T_g is observed. Experimentally, they have been determined by infrared spectroscopy by O'Reilly–Mosher [39], Grohens [40], and Tretinnikov [41]. The conformational energies determined by Tretinnikov cannot be used in Eq. (7) since the 2-levels model cannot be applied. O'Reilly–Mosher's and Grohens results correspond to the model used to produce bond fractions (Eq. (8)), with no consideration of the excluded volume at short range. In the case of Grohens' data, E_{conf} is found to be equal to 0.471 and 0.879 kcal mol^{-1} for i-PMMA and s-PMMA, respectively. It should be pointed out that a slight difference in the E_{conf}/T_g ratio is observed between the two PMMA configurations. Numerical application of Eq. (7) yields values of $\Delta C_{\text{conf(shape)}}$ of 0.011 and 0.025 J/(g K) for i-PMMA and s-PMMA, respectively. These values have then to be multiplied by the number of beads, 5.9, which corresponds to the ratio of the volume of a repeat unit to the volume of a CH_2 unit, and the number of flex bonds to reach the experimental values of $\Delta C_{\text{conf(shape)}}$ as indicated by DiMarzio and Dowell [37]. To extract the number of flex bonds, the experimental value of $\Delta C_{\text{conf(shape)}}$ is determined by subtracting $\Delta C_{\text{vib.}}$ and $\Delta C_{\text{conf(vol.)}}$ from ΔC in Eq. (4), yielding 0.215 and 0.140 J/(g K) for i-PMMA and s-PMMA respectively (Table 3). Consequently, the numbers of flex bonds are 3.35 and 1.00 respectively. Using the values of conformational energy determined by O'Reilly–Mosher, lower number of flex bonds per repeat unit have been determined: 1.7 and 0.4, respectively [39]. These small numbers can be explained by different experimental conditions. Moreover the E_{conf}/T_g ratio was found to be different for the two PMMA configurations, which has been stated to be equal by O'Reilly [17]. Nevertheless, in all cases i-PMMA exhibits the higher number of flex bonds. A higher number of flexes for the isotactic configuration indicates that more bonds are needed to yield change in the shape of the chain, involving a higher stiffness for this configuration. Such a result is not surprising since the characteristic ratio of i-PMMA, 11.2, is higher than for s-PMMA, 7.5 [42].

From an atomistic simulation viewpoint, the procedure used to determine experimentally $\Delta C_{\text{conf(shape)}}$ can no longer be used since Eq. (7) reveals the statistical behavior of polymer chains with temperature. The use of only 5 configurations, which explore a small domain of the phase space at each temperature (5 ns) is far from the thermodynamic limit. Despite this limitation, the simulated $\Delta C_{\text{conf(shape)}}$ was determined by subtracting $\Delta C_{\text{vib.}}$ and $\Delta C_{\text{conf(vol.)}}$, in the same way as the experimental one. AS actually yields very low values for $\Delta C_{\text{conf(shape)}}$ of 0.09 and 0.07 for i-PMMA and s-PMMA respectively. Due to errors stemming from the

Table 3
Experimental (30,000 g/mol) and simulated (300 RUs) contributions to the leap in the heat capacity stemming from Eqs. All values are in J/g.

PMMA	ΔC		$\Delta C_{\text{vib.}}$		$\Delta C_{\text{conf(vol.)}}$		$\Delta C_{\text{conf(shape)}}$	
	Exp.	AS	Exp.	AS	Exp.	AS	Exp.	AS
Iso	0.420	0.280	0.087	0.074	0.118	0.116	0.215	0.090
Syn	0.360	0.260	0.102	0.078	0.118	0.115	0.140	0.067

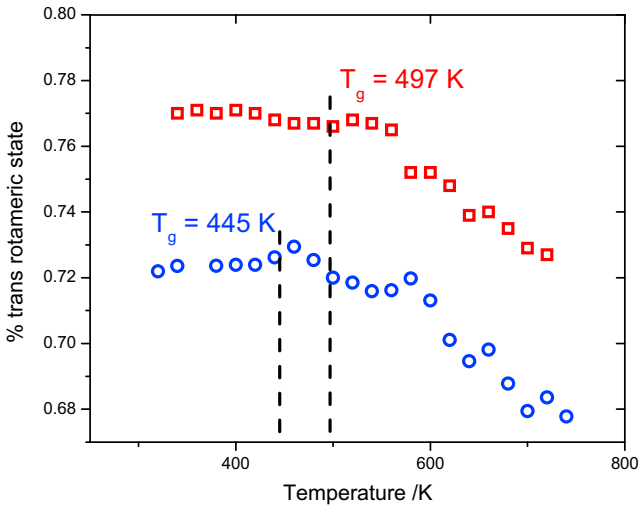

Fig. 6. Percentage of the trans rotameric state of one configuration of i-PMMA (○) and s-PMMA (□) versus temperature.

determination of the different heat capacities, analysis of these very low values is delicate. Nevertheless, since the contribution of $\Delta C_{\mathrm{conf(shape)}}$ to the total heat capacity represents the change in the rotameric states, the percentage of the *trans* rotameric state $(1-f)$ of i- and s-PMMA has to be regarded.

The variations of the trans rotameric state, t, with respect to the temperature for only one configuration of i-PMMA and s-PMMA are shown in Fig. 6. These curves disclose the freezing of the rotation of bonds along the polymer chain at T_g. Rotations between rotameric states along the backbone at temperatures above T_g are thus observed using AS. However, the percentage of the trans rotameric state is not compatible with experimental data since $\Delta C_{\mathrm{conf(shape)}}$ exhibits a very low value compared to the experimental data (Table 3). The freezing is thus clearly expressed but the discrepancy in $\Delta C_{\mathrm{conf(shape)}}$ reveals that this percentage is not accurate. Accordingly variation in rotameric states occurring at the glass transition is not completely depicted by full atomistic molecular dynamics simulation.

4. Conclusion

The domain of time covered by atomistic simulation (AS) is on the order of 10 times lower than the experimental one. Despite this very reduced momentum space explored by AS, a variation in the slope of the specific volume is observed by decreasing the temperature. By studying this transition at different cooling rates, it has been shown that this transition temperature is related to the experimental T_g through the WLF equation. It was actually unanticipated that AS could reproduce so suitably this macroscopic property since all the degrees of freedom of a real polymer chain cannot be accurately reproduced using such small domains of time. The aim of this study was thus to discern the degrees of freedom that are correctly frozen at the glass transition. For that purpose heat capacity is reported with respect to the temperature, and simulated and experimental data are compared to a theoretical model of this transition. They reveal that despite an accurate description of the free volume expansion though the well-established William-Landel-Ferry (WLF) equation, and a freezing of the rotations in the backbone bonds, the change in the shape of the polymer conformation lacks of time to be accurately described. Actually, the duration of molecular dynamics is undoubtedly under the Rouse time. This limitation does not involve the non-representation of the phenomena occurring at the glass transition, but controls the actual analysis of data to only local properties. For instance, the study of diffusion requires longer times, but localized disturbances such as changes in the energy, internal parameters except dihedral angle, can be specifically regarded [43].

In a previous study, the Adam–Gibbs model was used to describe the glass transition determined by AS [8]. The next step of this study will be to determine the cooperativity length that is related to the entropy parameter that is found in the formula of the effective activation energy. The results that will be derived from this study will indicate if the limit of detection of the method is reached since an asymptotic value has to be attained as the duration of the molecular dynamics simulation increases.

Acknowledgment

The present work was supported by the Natural Sciences and Engineering Research Council (NSERC) of Canada, and Université de Sherbrooke. Computations have been made available thanks to the Canadian Fund Innovation (CFI), the Fonds Québécois de la Recherche sur la Nature et les Technologies (TQRNT) and Réseau Québécoise de Calcul Haute Performance (RQCHP). We thank Pr. E. Zysman-Colman for helpful discussions during the writing of the article.

References

[1] Angell CA. Proc Natl Acad Sci USA 1995;92(15):6675–82.
[2] Ngai KL. J Non-Cryst Solids 2007;353(8–10):709–18.
[3] Binder K, Baschnagel J, Paul W. Prog Polym Sci 2003;28(1):115–72.
[4] Rigby D, Roe R-J. J Chem Phys 1987;87:7285–92.
[5] Soldera A, Grohens Y. Macromolecules 2002;35(3):722–6.
[6] Soldera A. Macromol Symp 1998;133:21–32.
[7] Soldera A, Metatla N. Phys Rev E 2006;74(6):061803.
[8] Metatla N, Soldera A. Macromolecules 2007;40(26):9680–5.
[9] Adam G, Gibbs JH. J Chem Phys 1965;43:139–46.
[10] Ferry J. Viscoelastic properties of polymers. 3rd ed. New York: Wiley; 1980.
[11] Schmidt-Rohr K, Kulik AS, Beckham HW, Ohlemacher A, Pawelzik U, Boeffel C, et al. Macromolecules 1994;27:4733–45.
[12] Soldera A, Grohens Y. Polymer 2004;45(4):1307–11.
[13] Genix AC, Arbe A, Alvarez F, Colmenero J, Farago B, Wischnewski A, et al. Macromolecules 2006;39(18):6260–72.
[14] Karasz FE, MacKnight WJ. Macromolecules 1968;1(6):537–40.
[15] Soldera A. Polymer 2002;43(15):4269–75.
[16] Gibbs JH, Di Marzio EA. J Chem Phys 1958;28:373–83.
[17] O'Reilly JM. J Appl Phys 1977;48(10):4043–8.
[18] Tombari E, Ferrari C, Salvetti G, Johari GP. Phys Rev B 2008;78(17):176302.
[19] Cangialosi D, Alegria A, Colmenero J. Phys Rev B 2008;78(17).
[20] Soldera A, Metatla N. Internet electron. J Mol Des 2005;4(2005):721–36.
[21] Soldera A, Metatla N. Compos Part A Appl Sci Manuf 2005;36(4):521–30.
[22] Metatla N, Soldera A. Mol Simul 2006;32(14):1187–93.
[23] Theodorou DN, Suter UW. Macromolecules 1985;18:1467–78.
[24] Meirovitch H. J Chem Phys 1983;79(1):502–8.
[25] Jorgensen WL, Maxwell DS, Tirado-Rives J. J Am Chem Soc 1996;118(45):11225–36.
[26] Haile JM. Molecular dynamics simulation. New York: John Wiley & Sons; 1992.
[27] Berendsen HJC, Postma JPM, Van Gunsteren WF, DiNola A, Haak JR. J Chem Phys 1984;81:3684–90.
[28] Allen MP, Tildesley DJ. Computer simulation of liquids. Oxford: Clarendon Press; 1987.
[29] Plimpton S. J Comput Phys 1995;117(1):1–19.
[30] Chandler D. Introduction to modern statistical mechanics. New York: Oxford University Press; 1987.
[31] Soldera A, Dognon JP. Macromol Symp 1997;119:157–64.
[32] Tombari E, Ferrari C, Salvetti G, Johari GP. Phys Rev B 2008;78(14):144203.
[33] Strobl GR. The physics of polymers: concepts for understanding their structures and behavior. 2nd ed. New York: Springer-Verlag; 1997.
[34] Wunderlich B. Thermal analysis of polymeric materials. Berlin: Springer; 2005.
[35] Pyda M, Bopp RC, Wunderlich B. J Chem Thermodyn 2004;36(9):731–42.
[36] Pyda M, Wunderlich B. Macromolecules; 1999:2044–50.
[37] DiMarzio SF, Dowell F. J Appl Phys 1979;50(10):6061–6.
[38] Sundararajan PR. Macromolecules 1986;19:415–21.
[39] O'Reilly JM, Mosher RA. Macromolecules 1981;14:602–8.
[40] Grohens Y, Brogly M, Labbe C, Schultz J. Polymer 1997;38(24):5913–20.
[41] Tretinnikov ON, Ohta K. Macromolecules 2002;35(19):7343–53.
[42] Jenkins R, Porter RS. Polymer 1982;23:105.
[43] Langer J. Phys Today 2007;60(2):8–9.